# Valeology: International Journal of Medical Anthropology and Bioethics (ISSN 2995-4924) VOLUME 02 ISSUE 05, 2024

# PROPERTIES OF SOME FERRITE COMPOUNDS AND SPECTROSCOPIC PREPARED BY SOLID-STATE REACTIONS

Abdhu Same Fawzi Abdul Aziz, Shatha Nasser Abdul Rahman

Department of Physics, College of Science, University of Tikrit, IRAQ

# **Abstract:**

In this research, some ferrite compounds with chemical formulas (Mn0.5Zn0.5Fe2O4, Ni0.5Zn0.5Fe2O4) were synthesized. Consecutively in a solid-state reaction method at a temperature of (1000 0 C) for (4 hours), the structural properties represented by the lattice constant (a), the theoretical density ( $\rho$  a), the density as a function of X-ray diffraction (p x-ray) and porosity p and the grain (D) in terms of the X-ray diffraction technique, as the results showed that all samples have a spin-cubic crystalline structure and that the lattice constant of the model (Mn 0.5 Zn 0.5 Fe 2 O 4) is greater than the two models (Co 0.5 Zn 0.5 Fe 2 O 4 and Ni. 0.5 Zn 0.5 Fe 2 O 4) respectively. The results also showed that the density as a function of the X-ray diffraction technique for the model (Ni 0.5 Zn 0.5 Fe 2 O 4) is greater than the density of the compound (Co 0.5 Zn 0.5 Fe 2 O 4), which is considered denser than the compound (Mn 0.5 Zn 0.5 Fe 2 O 4) This result will contribute to an increase or decrease in permeability (P) and grain size (D) resulting from the differential trend of Miller coefficients (220) and for all models, as the largest value is for the model(Ni 0.5 Zn 0.5 Fe 2 O 4) while it is smaller for the two values Co 0.5 Zn 0.5 Fe 2 O 4, Mn 0.5 Zn 0.5 Fe 2 O 4, respectively. The surface topography was also studied according to the scanning electron microscope (SEM) technique, while the properties The isolation of all models, represented by the dielectric constant, both real ( $\varepsilon$  1) and imaginary ( $\varepsilon$  2) It was shown that the amplitude decreases with frequency due to the process of electrical polarization. In addition, energy dispersive X-ray spectroscopy (ADEX) was studied for all samples. The results showed that the percentage of oxygen content is high in all samples, but it is noted that the percentage of zinc is less than the equivalent percentage within the spinel structure. Ferrite, Also, for all models, it was shown that there is an inverse relationship for frequency and amplitude with both the real  $(\varepsilon 1)$  and imaginary (2ε) dielectric constant.

**Keywords:** Ni-Zn ferrite; Mn-Zn ferrite; Structural properties; CO-Zn ferrite; dielectric constant solid state reaction method.

#### Introduction

Ferrite is considered one of the materials with continuous development, which makes it the focus of attention of many researchers recently because of its unique properties, as ferrite is produced by traditional methods that require high temperature. Ferrite has the general formula Mfe<sub>2</sub> O <sub>4</sub>, whereM represents the divalent metal elements. like) (Mn <sup>+2</sup>, Ni <sup>+2</sup>, Co <sup>+2</sup>, ...... As for their classification based on the crystal structure, they are classified into three types: hexagonal ferrite, cubic ferrite) and garnet ferrite. Compounds make them used in the construction of electronic devices that include circuits that operate at high and low frequencies [1]. The compositional, insulating and spectral properties are studied. Interest in ferrite has appeared in several fields of technology and science, as it is used in transformer cores, antenna bars, deletion coils [2-3], and circuits. Integrated magnetic resonance imaging (MRI) [4]

### Experimental details

# > Sample preparation methods

(NiO, CoO, MnO, Fe 2 O 3, ZnO 2) with purity degrees ranging from (98-99%) were used in Preparation of ferrite compounds with chemical formulas (Co 0.5 Zn 0.5 Fe 2 O 4, Mn 0.5 Zn 0.5 Fe 2 O 4, Ni <sub>0.5</sub> Zn <sub>0.5</sub> Fe <sub>2</sub> O <sub>4)</sub>, which are called A, B, and C, respectively, by the solid-state reaction method. Models using the raw materials mentioned previously and in the same weight ratios indicated in the chemical formulas of the compounds were taken using a sensitive arithmetic balance (4<sup>-10 grams)</sup>, then these materials were mixed together using an agate mortar and ground well to obtain a homogeneous mixture for 3 hours) (Then it is sintered At a temperature of 700 °C for 4 hours using an electric oven to remove the impurities in it. The mixture is re-grinded for (0.5 hours) To become more homogeneous, it will be sieved to obtain fine grains During the sifting process, the binder polyvinyl alcohol (PVA) is added to it, and then the resulting powder is placed in a stainless steel mold with a diameter to compress the samples using a hydraulic press for 5 minutes under pressure (5 tons). Then the samples are heated again at a temperature of (1000 <sup>0</sup> C) for a period of (4 hours) to obtain the final models, after which we leave the samples to cool at room temperature, and finally we will obtain solid discs with a smooth surface for the purpose of studying the structural properties of Balala X-ray diffraction technique model) PW1730 within the range (2  $\theta$  =20  $^{0}$  -80  $^{0}$ ) as well as studying the properties Isolation as a function of LCR-meter technology.

#### Structural characteristics

The X-ray diffraction technique is of great importance in studying the structural properties of samples at the atomic level [5-7], as the crystal system of the samples was identified by calculating the interstitial distances between the atomic levels through Braak's law. It is known that X-rays are an electromagnetic ray with a short wavelength. Within the range  $(0.1 - 10^{-0} \text{ A})$  to achieve Braak's law d hkl  $\leq \lambda$  According to the following mathematical relationship [10-6]

```
n \lambda = 2d_{hkl} \sin \theta.....(1)

n = Diffraction order

\lambda = Wavelength of X-rays (1.5418A ^{0)}
```

(a) was also calculated for all models through the mathematical relationship of the cubic crystal system <code>]11[</code>

$$d_{hkl}=a/(h^2+k^2+l^2)^{1/2}$$
....(2)

a =unit lattice constant

 $\theta$  = diffraction angle

 $d_{hkl} = =$  Distances between crystal planes

Hkl= Miller coefficients

While the crystal size was calculated according to the Debye-Scherer equation [12]:

D=  $0.9\lambda\beta.\cos\theta...$ (3)

D= Crystal size

B= greatest midpoint which is converted to the radial angle by multiplying by  $\pi/180$ 

As for calculating the density in terms of X-ray diffraction, it was calculated according to the relationship (4) ] 13 [

P = Z.MwtV.NA....(4)

unit cell density of the reticle =  $\rho$ 

Z= number of molecules per unit cell (Z=8)

Mwt= molecular weight of the compound

V= unit cell volume = a3

N  $_{A=_{\rm l}}$  number of avocado 6.023×10  $^{23}\,mol$   $^{\text{--}1}($ 

The physical density of all models was also calculated according to the mathematical relationship

$$\rho_a = m V.....(5)$$

Density The phenomenon (b): is Density Measured Experimentally Of the results X-ray diffraction XRD

Density The real one (s): is Density Practically measured from the mass and size of the sample, as the size of the capsules is calculated from the size of the cylinder from the thickness and diameter of the samples.

And it was done account porosity (Porosity) for samples prepared by solid-state reactions using Formula The following, as shown in Tabl: 2 [14]

Well done account distance In-betweenness For ions Magnetism in location Quadrant Surfaces A  $L_{A)}$  and distance between ions Magnetism in location Eight Surfaces B ( $L_{B)}$  using The two relationships [15]

LA=3a4 ..... (7 a)

LB=3a2.....(7 b)

#### Results and discussions:

Figure (1) indicates the X-ray diffraction patterns for compounds A, B, and C, respectively, as it is clear from the following figure a change in the Braak angles and that the Miller coefficients that were reached are practically identical to the international cards found, (card No CO 15-0806), (card No Mn 23-1237) (card No of Ni 078-0753) respectively

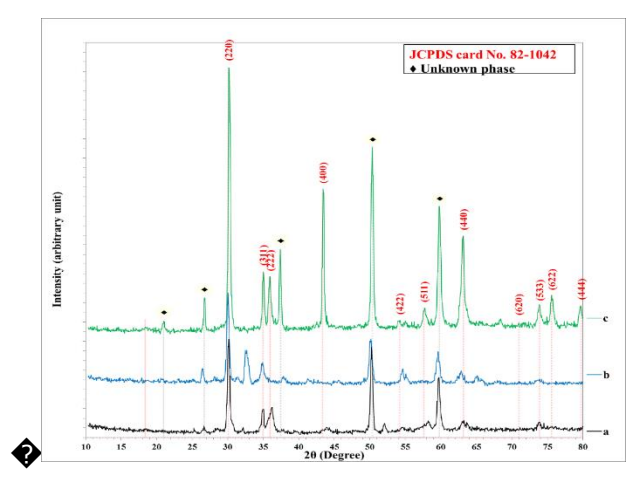


Figure 1: X-ray diffraction patterns of metal ferrite samples (A) (B) And (C) Straight and prepared by solid-state reactions

Figure 1 also shows the values of X-ray diffraction angles and the width of the peaks ( $\beta$ ). As well as the appearance of additional peaks due to the failure to achieve a pure composition of the metal ferrite due to incomplete homogeneity, which is due to its preparation using the method of solid state reactions because the ions within the powder do not reach every point in a homogeneous manner according to the ratios used. As for Table (1) It refers to the most important scientific calculations that were reached when studying the structural properties represented by the lattice constant, the grain size, and the density as a function of X-ray diffraction and the length of the interfacial distances for the tetrahedral and octahedral sites of the models A, B, and C, respectively, as well as the grain size as a function of the Debye-Scherrer relationship.

Table 1 : Reticle constant a), reticle volume V, calculated density ( $\rho_x$ ), and values of L A and L B For ferrite metal samples A, B, and C, respectively, prepared by solid-state reactions

Sample	a(Å)	V(Å 3)	$\rho$ (gm/cm <sup>3)</sup>	$L_{A}(^{0}A)$	$L_{B(^{0}A)}$	D(nm)
A	8.4195	596.841	5.294	3.646	7.292	20.64
В	8.4245	597.905	5.240	3.648	7.296	23.625
С	8.4054	593.848	5.318	3.640	7.279	26.02

It is clear from the previous table that there are clear changes in the values of the inter-distance of the tetrahedral and octahedral sites, as these changes are attributed to the replacement of the Zn  $^{+2}$  ion with metal ions Mn  $^{+2}$ , CO  $^{+2}$ , Ni  $^{+2}$ , respectively. The values of the atomic radius are due to these CO  $^{+2}$  >Ni  $^{+2}$  >Mn  $^{+2}$  >Zn  $^{+2}$  The reason for the change in the values of the lattice constant for all models is due to the difference in density as a function of X-ray diffraction. As it is known that porosity depends on density according to the relationship mentioned previously, its value will change as is. It is shown in Table (2), which in turn contributes to clarification Lengths Jumping Ionic  $L_A$  And  $L_B$  because Replacement of zinc ions with metal ions of different ionic diameters structure - Farita 16It turns out that the relationship between the ionic radius and the lattice constant is direct, where the ionic radius is arranged Crystalline lacoxide elements used)  $r_{Mn} > r_{Zn} > r_{Co} > r_{Ni}$  ]17 [ . It appears from Table 1 Change length values all from  $L_A$ ,  $L_B$  according to the dimensions of the mesh due to the direct relationship between them, so that they are as large as possible for sample B and as small as possible for sample C. While We note that the crystalline size of sample C is larger And less than B, A, respectively.

Table 2 shows the calculated theoretical density of the material and that calculated from XRD, and the true density For ferrite mineral samples A and BC, respectively

Technique	Sample	$\rho_b (gm/cm^{3)}$	$\rho s (gm/cm^{3)}$	Porosity
	A	5.294	4.256	19.605
Powder	В	5.240	4.329	17.392
	C	5.318	4.184	21.337

It is clear from Table 2 that the degree of porosity decreases with the efficiency of compaction of samples during powder compaction, which depends on the size of the particles used. While the value of porosity varies slightly from one sample to another depending on the type of compensation element due to the different melting points of the components used, we note that the most porous of them is sample C compared to the other samples A, B, respectively.

# **Surface Topography**

Figure 2 shows the surface morphology of models A, B, and C, respectively, using ... Microscope Email Field effect scanner (FE-SEM) when power Zoom (35kx As it turns out that Sample A is a blend product Two substances are CO and Zn. It is also clear from the figures that particles Ferrite is agglomerated in shapes big It is compact, and its diameter ranges up to 835 nm And the result on Growth of its crystal structure during The process of sintering the samples at a temperature of (1000) <sup>0</sup>C) for a period of 4 hours. As the previous pictures show the presence of cavities and grooves, the process of compacting the sample is incomplete. In addition, another phase appeared, consisting of relatively small spherical particles closely packed together. While Replacing half of the Zn <sup>+2</sup> atoms with Mn <sup>+2</sup> instead of CO <sup>+2</sup> led to the appearance the sample More compact, where it clumps Molecules Ferrite in shapes big It has a lamellar structure, which goes back to the spinel-ferrite structure As shown by previous studies [18]. The sample appears more compact, meaning it has less porosity. Due contrast Degree of compaction For samples with Change the type of metal replaced to Difference in the melting point of different metals (Co  $^{+2}$  = 1246  $^{\circ}$  C, Mn  $^{+2}$  = 1495  $^{\circ}$  C). In addition, another form of relatively small spherical particles appeared, with a diameter of about 180 nm, stacked together. The appearance of two forms of particles confirms the presence of two phases within the composition of the samples prepared by solid-state reactions, as I showed Results of Xray examinations.

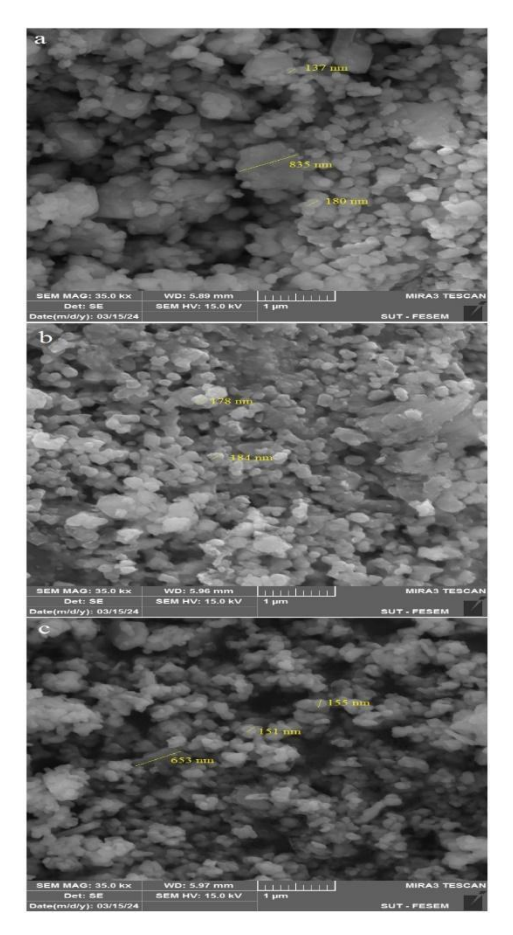


Figure 2: The pictures Samples (A, B, and C) as measured by the scanning electron microscope

As it shows that Figure 3 Spectra ADEX For models A, B, C respectively. We note the availability intensity Tops emissions Visions value around content Elements existing inside Samples. And it shows Spectra Many from Peaks the interview For lines emission Elements Component For the boat Which Zinc (Zn <sup>+2)</sup>, iron (Fe <sup>+2)</sup>, and oxygen (O <sup>-)</sup> in addition to Elements Co <sup>+2</sup> compensation, Mn <sup>+2,</sup> Ni <sup>+2</sup> in Her samples . In addition to that, He appears summit Emission when 2.1 keV, And it arises from layer gold Kind that Failed on Samples when Prepare it To check Microscope Email from Okay more Accuracy Pictures that Results that It was completed Get on her from analysis samples, as he Explained in schedule 2 mentioned previously that rate content Oxygen High in all samples, But notice that rate an item Zn <sup>+2</sup> less from The ratio Reward inside structure Spinel - ferrite. He is consoled difference rate Oxygen O <sup>-2</sup> from a sample to Other to difference in degree oxidation For items different.

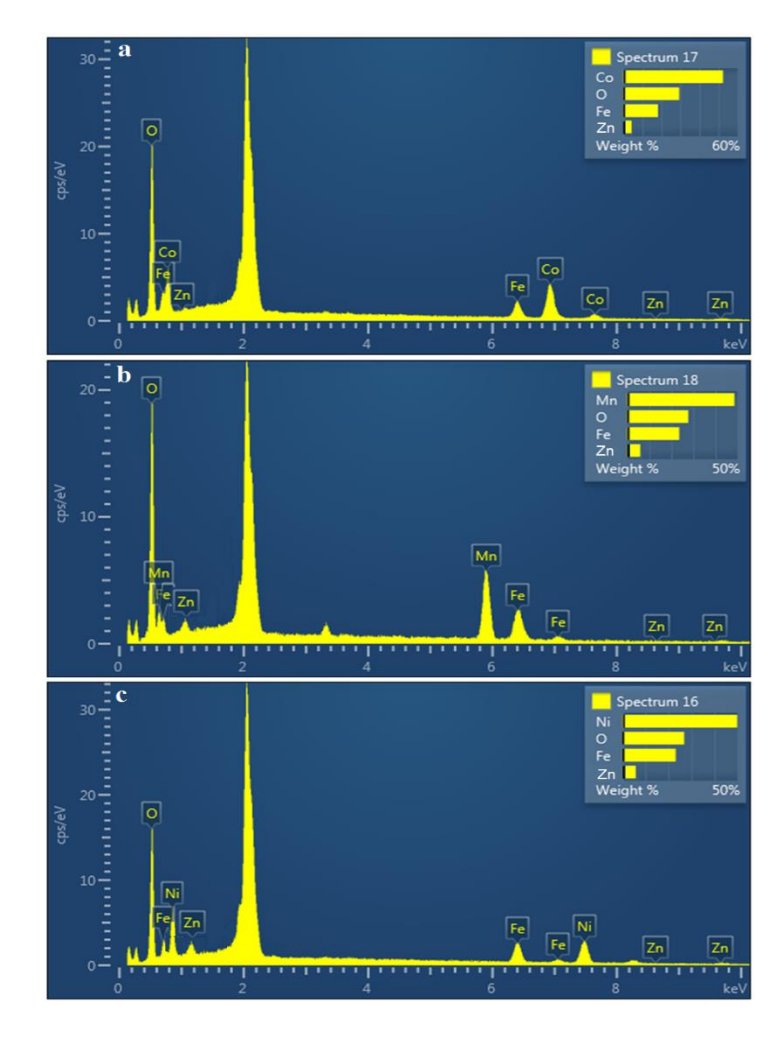


Figure 3: ADEX dishes For models A, B, and C respectively

# **AC** electrical conductivity (**AC** conductivity)

Show Figure 4 The relationship between Logarithm of conductivity electrical alternating A.Cwith Logarithm Frequency Angular  $\omega$  samples A, B, C respectively Through which the relationship between alternating conductivity and frequency was determined. The curves show the natural behavior of the alternating conductivity change as it increases with The frequency increases and this behavior indicates that the samples under study are semi-conducting materials. As the relationship seemed Nearly linear within the frequency range 75 to 550 kHz . is calculated The Worker Exponential (s) of Mile Region Sin By relationship:

$$ln[fo](\sigma A.C)=s ln[fo]()$$
 .....(8)

It is shown in Table (3). As it appears from the figure, there is a difference in Connectivity the current Alternating between Samples different According to the compensation component where It appeared to be the least for the sample doped with CO <sup>+2</sup>, and it increased with Mm <sup>+2</sup>, and it increased more with nickel . The difference in conductivity of the samples is due to the difference in the optical energy gap, because a decrease in the energy gap leads to an increase in electrical conductivity

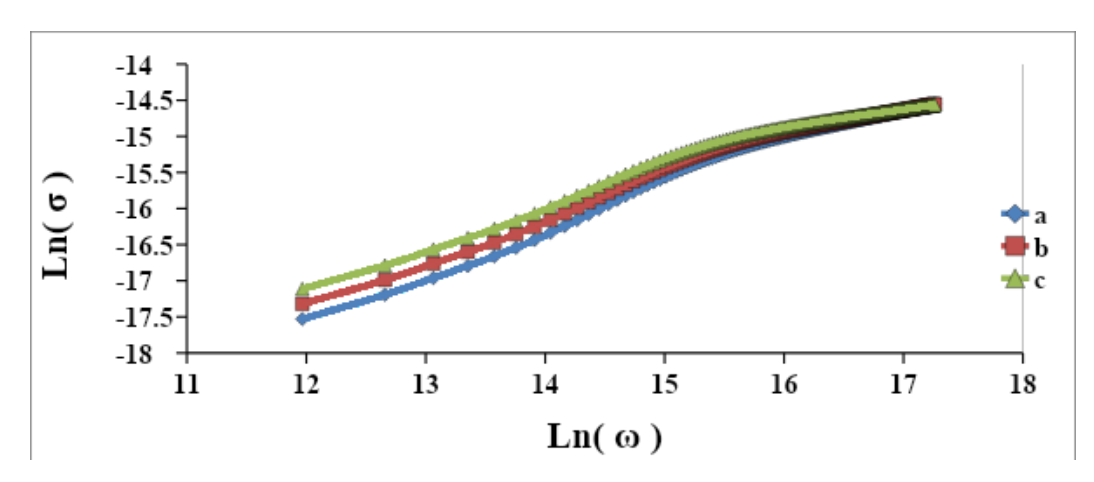


Figure 4: Change of  $\ln \sigma$  with  $\ln \omega$  for models A, B, and C, respectively

Schedule 3: The value of the exponential factor (s) for samples A, B, and C, respectively

	A	В	C
Powder	0.742	0.696	0.647

While Figure (5) shows a change Capacity with Frequency 1 l samples A, B, C respectively Which shows a decrease Capacity with Frequency because of practical polarization The electrician

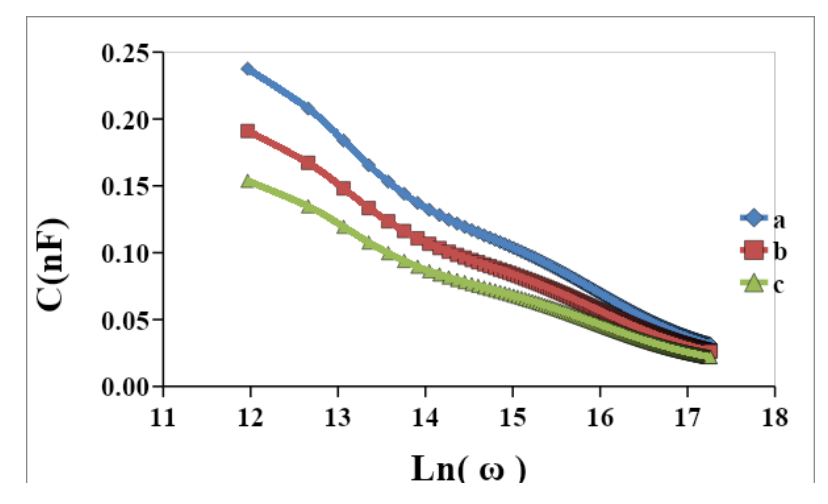


Figure 5: Change of electrical capacitance with ln ω for samples A, B, and C, respectively

While it was found that constant Insulation The true electrode ( $\epsilon_{1}$ ) for the three samples with Frequency Dielectric constant curves have the same behavior With capacity because they are They are proportionate . when study Changes Fixed Insulation with frequency, observed that The value of  $\epsilon_{1}$  Go down With an increase Frequency . This was explained because drop value Fixed Insulation with Frequency from during Operations polarization Different.while noticing That  $_{2\epsilon}$  decreases with more Frequency For all samples in particular when Frequencies Low Because of migration ions from Electrodes electrical . And at Frequencies The high Prepare Vibration Ionic It is a source Loss Insulation The electrician] 19 [. While we note that the values of  $_{2\epsilon}$  For her three samples Behavior Oppositely About  $_{1}$   $\epsilon$  The values of  $\epsilon_{2}$  increase by changing the compensation element from CO  $^{+2}$  to Mn  $^{+2}$  and then Ni  $^{+2}$ 

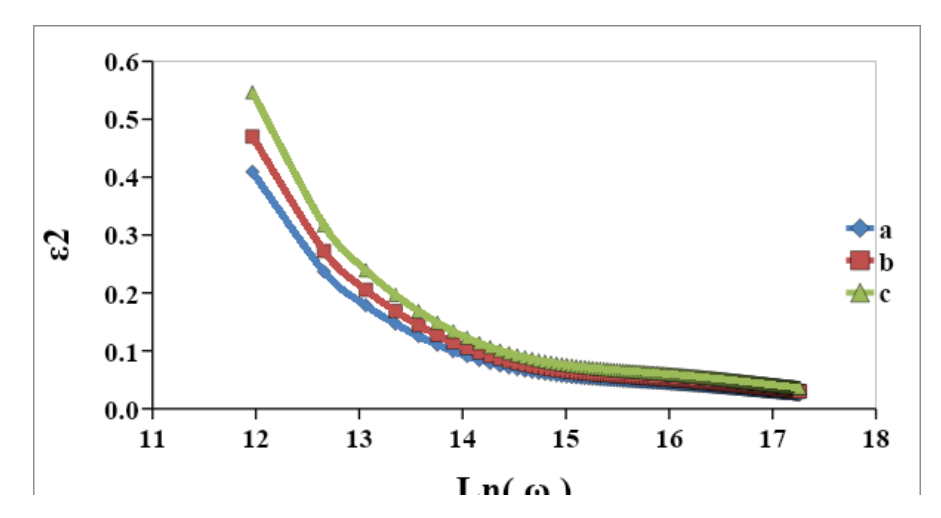


Figure 6. Variation of the imaginary dielectric constant with  $\ln \omega$  for the samples A, B, C respectively

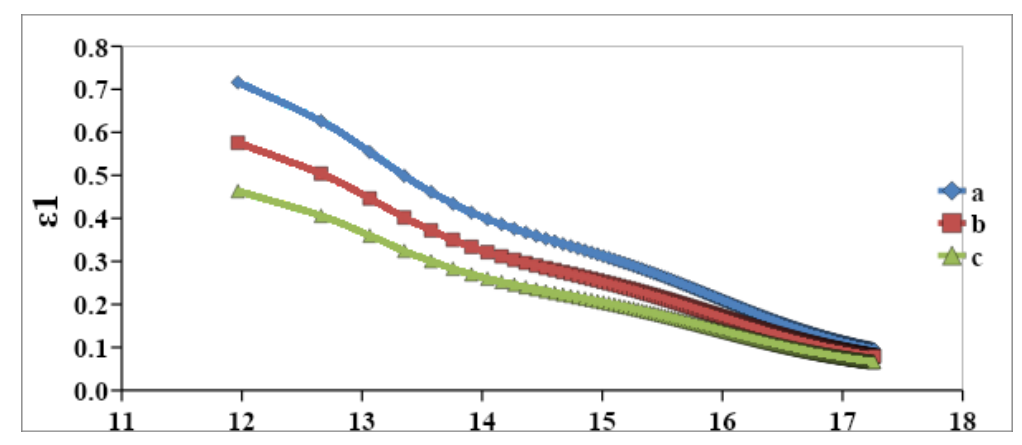


Figure 7: Change of the true dielectric constant with  $\ln \omega$  for the samples A, B, C respectively Conclusions:

- 1. All models showed that they have a cubic crystal structure
- 2. To change Fixed the network And size cell And lengths Jumping Ionic (L A, L B for the composition of ferrite based on the ionic radius of the substitute element instead of zinc, which Turn impact In a way big on Properties The compound
- 3. Electron microscope images showed a difference in the nanostructures of the surfaces of the models, which are more porous. It appeared solid and without surface cavities. This result was confirmed by porosity calculations based on the apparent and actual density of the samples.
- 4. The real and imaginary insulation constant decreases with increasing frequency for all model.

#### References

- 1. H.K. Bowen, D.R. Human & W. Gingery "Introduction to ceramics", 2nd Edition, John Wiley and Sons, New York (1976).
- 2. Kumar," Development of Ni Zn nanoferrite core material with improved saturation magnetization and DC resistivity" J. Magn. Magn. Mater. 320, 1995- 2001 (2008).
- 3. Hwang, Y." Microwave absorbing properties of Ni Zn ferrite synthesized from waste iron oxide catalyst" Mater. Lett. 60, 3277-3280 (2006).
- 4. Yan," Characterization and low-temperature sintering of Ni0.5Zn0.5Fe2O4 nano-powders prepared by refluxing method" Powder Technol. 92, 23-26 (2009).

- 5. Ahmed Maqsood, Mohammed Jamal, "Mater. Science and Engineering", 139, PP. (164)-(170); (2007).
- 6. Mohammed Abdul khaddar, J. Jacob, "A. Ponapean and K.T Mathew Microwave Dielectric Properties of Nanostructured Nickel Ferrite", Bull. Materials Sci., Volume 31, Number 6, PP.(847)- (851),(2008).
- 7. ليمى عبد السالم, حذامة عبد, رعد أحمد" تأثير درجة حرارة التمدين عمى خصائص الكهربائية للفرايت المرن (402Fe0.8Zn0.2Ni)
- 8. B. K. Chougule and P. U. Mahamuni, "Structural Magnetic an Dielectric Properties of Nano crystalline Ni-Zn Ferrites", Scholar Research Library, Volume 1, Number 1, P. (112 118), (2010).
- 9. A. Lagashetty, A. Mbhavikatti, & S. Kulkarni; "Electromagnetic Studies of Nickle Ferrite Synthesized by Microwave route", International Journal of Technology and Engineering Science, Volume 3, Number 1, PP. (687)- (693), (2011).
- 10. فرايت", مجمة إبن الهيثم لمعموم ( Ni-Mn) في الخواص الفيزيائية والعزلية لممركب ( 2SiO) عباس كريم, "تأثير السميكا .10 التطبيقية والعموم الصرفة, مجمد )22(, العدد )9(, صفحة )080-800(.
- 11. K. Jalaiah, K. C. Mouli, K. V. Babu, and R.V. Krishnaiah, "Structural, electrical and magnetic properties of Mg-Zr co-substituted Ni0.5Zn0.5Fe2O4," J. Sci. Adv. Mater. Devices, vol. 4, pp. 310–318, 2019.\
- 12. S. Kahraman, S. Çetinkaya, S. Yaşar, and İ. Bilican, "Polyethylene glycol-assisted growth of Cu 2 SnS 3 promising absorbers for thin film solar cell applications," Philos. Mag., vol. 94, no. 27, pp. 3149–3161, 2014.
- 13. L. Glasser and H. D. B. Jenkins, "Lattice Energies and Unit Cell Volumes of Complex Ionic Solids," J. Am. Chem. Soc., vol. 122, no. 4, pp. 632–638, 2000.
- 14. C. Rath, S. Anand, R. P. Das, K. K. Sahu, S. D. Kulkarni, S. K. Date, and NC. Mishra, "Dependence on cation distribution of particle size, lattice parameter, and magnetic properties in nanosize Mn-Zn ferrite," J. Appl. Phys., vol. 91, no. 3, pp. 2211–2215, 2002.
- 15. R. Tiwaria, M. De, H. S. Tewari, and S.K. Ghoshal, "Structural and magnetic properties of tailored NiFe2O4 nanostructures synthesized using auto-combustion method," Results Phys., vol. 16, p. 102916, 2020.
- 16. G. Mei-Zhen, Z. .Feng, L. Jing, and S. .Hui-Na, "Effect of annealing conditions on properties of sol-gel derived Al-doped ZnO thin films," J. Chinese Phys. Lett, vol. 26, pp. 1–7, 2019.
- 17. P. Chatterjee and A. K. Chakraborty, "Band-gap engineering of tungsten oxide nanoplates by cobalt ferrite co-catalyst for solar water oxidation," Opt. Mater. (Amst)., vol. 111, p. 110610, 2021.
- 18. C. Rath, S. Anand, R. P. Das, K. K. Sahu, S. D. Kulkarni, S. K. Date, and N.
- 19. A. Tataroğlu, "Dielectric permittivity, AC conductivity and electric modulus properties of metal/ferroelectric/semiconductor (MFS) structures," Gazi Univ. J. Sci., vol. 26, no. 3, pp. 501–508, 2013.